

Scanning tunneling spectroscopy of superconductivity on surfaces of $\text{LiTi}_2\text{O}_4(111)$ thin films

Yoshinori Okada¹, Yasunobu Ando², Ryota Shimizu¹, Emi Minamitani², Susumu Shiraki¹,
Satoshi Watanabe² & Taro Hitosugi^{1,3}

¹Advanced Institute for Materials Research, Tohoku University, Sendai 980-8577, Japan

²Department of Materials Engineering, The University of Tokyo, Tokyo 113-8656, Japan

³School of Materials and Chemical Technology, Tokyo Institute of Technology, Tokyo 152-
8552, Japan

Abstract

Unique superconductivity at surfaces/interfaces, as exemplified by $\text{LaAlO}_3/\text{SrTiO}_3$ interfaces, and the high transition temperature (T_c) in ultrathin FeSe films, have triggered intense debates on how superconductivity is affected in atomic and electronic reconstructions. The surface of superconducting cubic spinel oxide LiTi_2O_4 is another interesting system because its inherent surface reconstructions add complexity to superconducting properties. Investigations of such surfaces are hampered by the lack of single crystals or high-quality thin films. Here, we report the first spectroscopic evidence of a suppressed T_c on a surface of LiTi_2O_4 (111) epitaxial thin film. Low-temperature scanning tunneling microscopy has revealed an unexpected small superconducting energy gap and a large coherence length on the surface. Together with first-principles calculations, we find that a pseudogap opening at the Fermi energy modifies the surface superconductivity. Our results open a new direction of research, that of exploring anomalous superconductivity on the surface of *cubic transition-metal oxides* where the electronic states are spontaneously modulated.

Introduction

Recent advances in the atomic-scale synthesis and characterization of two-dimensional superconductors have kindled significant interest in their exotic electronic, orbital, and magnetic structures¹⁻⁶. In addition to the ultrathin superconducting films on substrates⁷⁻²⁰, surfaces of cubic-structure superconducting transition-metal oxides provide another interesting platform, because the spontaneous electronic and atomic *reconstructions* on surfaces modify superconductivity. A particularly interesting system is the spinel oxide (AB_2O_4) superconductor. In this system, the cubic pyrochlore sub-lattice of B-atoms provides large degeneracy (frustration) of charge-, spin-, and orbital-states in bulk^{21,22}, and a prominent degeneracy lifting at the surface is expected to lead rich electronic states on the surface. None of the previous studies, however, has revealed the electronic signature of modulated superconductivity on their surfaces.

Lithium titanate, $LiTi_2O_4$, is the only oxide superconductor with spinel structure²³⁻²⁶, and exhibits the highest transition temperature T_c (~ 13.7 K) of any spinel superconductors²⁷⁻³². It is known as a $3d^{0.5}$ metallic system (one half of an electron per Ti atom resides in the 3d states), and medium-coupling Bardeen–Cooper–Schrieffer (BCS) superconductivity with *s*-wave pairing symmetry has been proposed³³⁻³⁶. Recent transport data with epitaxial films showed an angle-dependent anomalous magnetoresistance, which is possibly related to a spin-orbital fluctuation effect³⁷. Based on this data, the similarity between $LiTi_2O_4$ and high- T_c cuprates has been discussed³⁷. Although superconducting properties of bulk $LiTi_2O_4$ have been investigated extensively, studies of the superconductivity at $LiTi_2O_4$ surfaces have been hindered by the lack of single crystals and high-quality thin films. Recently, high-quality epitaxial $LiTi_2O_4$ thin films

were successfully grown using pulsed laser deposition (PLD)^{38–40}; however, investigations of the superconductivity on LiTi₂O₄ surfaces remain unexplored. Accordingly, we have developed a scanning tunneling microscope combined with a PLD system⁴¹ to examine details of the LiTi₂O₄ surface *in situ* without exposing the surface to air.

Here, we report that a T_c is suppressed at the surfaces of LiTi₂O₄(111) epitaxial thin films, using scanning tunneling microscopy/spectroscopy (STM/STS) and first-principles density-functional theory (DFT) calculations. From the first atomic-scale observations of superconductivity on oxides with inherent 3D crystal structure, including perovskites and spinel oxides, we present measurements of the superconducting gap Δ and the coherence length ξ that indicate a modified superconductivity on the surface. We reveal that the suppressed T_c is induced by a pseudogap opening in the density of states (DOS) at the Fermi energy (E_F). These results therefore provide the first spectroscopic evidence of superconducting modification on the surface of cubic spinel oxides, paving a path to explore exotic superconductivity.

Results

Atomic-scale order on LiTi₂O₄ (111) film surface. We observed on the atomic level a well-ordered triangular lattice (Fig. 1a) on films grown using PLD with substrate temperature of 300°C, followed by an annealing in vacuum at 600°C. Magnetization measurements revealed that the T_c of the films were ~13 K (Fig. S1). In the close-up image (Fig. 1b), strong topographic corrugations (shown in blue) are observed together with weak topographic corrugations (shown in red), displaying 3-fold symmetry. This is consistent with the inherent 3-fold rotational symmetry along the [111] axis in a spinel system. The unit cell size was found

to be ~ 0.6 nm (Fig. 1b), which was independent of the location and sample bias voltages V_s . This size well matches that of the unit cell of LiTi_2O_4 bulk (111) plane. We concluded that the protrusions of the triangular lattice originate from Ti atoms on the surface, as discussed later.

Small $2\Delta/k_B T_c$ value on surface. In addition to the atomic-scale corrugations, we observed clear signature of superconductivity in tunneling spectra measurements at 4.2 K. The spectra obtained at a wide energy region (from -130 meV to $+50$ meV) and a narrow energy region (from -4 meV to $+4$ meV) are shown in Fig. 2a and b, respectively. To evaluate the superconducting gap Δ quantitatively, we analyzed tunneling spectra using the Dynes formula⁴² convoluted with an energy derivative of the Fermi–Dirac function F ,

$$\frac{dI}{dV}(eV_s, T) = \int_{-\infty}^{+\infty} \left\{ -\frac{dF(E + eV_s, T)}{dE} \right\} \times (a + bE) \times \text{Re} \left\{ \frac{E - i\Gamma}{\sqrt{(E - i\Gamma)^2 - \Delta^2}} \right\} dE$$

Here, we assume that the normal-state DOS near E_F has a linear dependence with energy E , expressed as $(a+bE)$, and Γ is the spectral broadening factor originating from a finite lifetime of a quasi-particle. The fitting parameters a , b , Δ , and Γ are determined with fixed temperature $T=4.2$ K. We fitted our spectra (Fig. 2b) with a single-component isotropic pairing gap, and we obtained $\Delta = 1.716 \pm 0.004$ meV and $\Gamma = 0.321 \pm 0.004$ meV. According to the BCS gap function, assuming the same T_c for surfaces and bulk (13 K), the obtained Δ value can be regarded as a gap value in the $T=0$ K limit. Importantly, with using bulk T_c , the obtained $2\Delta/k_B T_c$ value of 3.0 is unexpectedly small. In contrast, the $2\Delta/k_B T_c$ values reported in *polycrystalline* LiTi_2O_4 samples range from 3.5 to 4.0 in point-contact spectroscopy^{22,35,36} and Andreev reflection³⁷. A recent report using *epitaxial* LiTi_2O_4 thin films claims $2\Delta/k_B T_c = 4.07$ from point-contact spectroscopy²², and thus the obtained value of 3.0 is much smaller than that

of all the previous reports. Furthermore, the present value is even smaller than that for the weak coupling limit for s -wave BCS superconductivity of 3.52. As we shall discuss later, the origin for this unexpectedly small $2\Delta/k_B T_c$ is a pseudogap formation (reduced DOS at E_F due to partially gapped electronic states) on the surface (red-shaded area in Fig. 2b).

Long coherence length ξ on surface. To further study the origin of the modified superconductivity on the surface, we investigated the value of ξ from the electronic structures around a magnetic vortex core. We first analyzed the V_s dependent conductance (dI/dV) map around a single vortex core by applying an external magnetic field of 1.5 T perpendicular to the surface at 4.2 K (Fig. 3a–e). At $V_s = -8$ mV and $+8$ mV, we observed uniform conductance over the scanned region (Fig. 3a,e), whereas conductance values were depressed around the center of images at $V_s = -4$ mV and $+4$ mV (Fig. 3b and d). This depressed conductance is a consequence of suppressed coherence peaks. In contrast, the conductance map at $V_s = 0$ mV clearly represents enhanced conductance in the center region (Fig. 3c). This enhanced zero bias conductance around the center region is because of pair breaking. These energy evolutions of conductance map indicate signatures of a vortex core (Fig. 3a–e), and indeed, the evolution of tunneling spectra along line A–B in Fig. 3a clearly shows a typical spatial evolution of spectral shape across a vortex core (Fig. 3f).

To evaluate ξ , we analyzed the zero-bias conductance data as a function of the radial distance from the vortex core center r (Fig. S2). We first extracted the zero-bias conductance Z as a function of mean distance r . Then, we fitted the $Z(r)$ by the exponential decay function $Z(r) = Z(\infty) + A \exp(-r/\xi)$, where A is a constant and $Z(\infty)$ is the normalized zero bias conductance away from the vortex core⁴³. From the fitting, we obtained $\xi \sim 12 \pm 1$ nm (Fig. 3h). This value

is much larger than the ξ_{GL} values obtained from the upper critical field (H_{c2}) using the formula $H_{c2} = \Phi_0 / 2\pi\xi_{GL}^2$ (Φ_0 is the magnetic flux quanta) based on Ginzburg–Landau theory. For epitaxial LiTi_2O_4 thin films, the ξ_{GL} values estimated from macroscopic measurements are 4.1–4.7 nm^{39,44}. Whereas excellent agreement between ξ and ξ_{GL} values have been reported in other superconducting systems such as Fe-based superconductors^{43,45}, the values of ξ obtained on the *surface* of LiTi_2O_4 are much larger than the estimated ξ_{GL} obtained from transport measurement techniques. The deviation of ξ from ξ_{GL} also implies that there is a difference in superconductivity between surface and bulk.

Discussions

To understand the superconductivity on the LiTi_2O_4 (111) surface, we calculated the electronic structures of four possible bulk-cut surfaces: two-types of O-terminated, Kagome-lattice Ti-terminated, and TiLi_2 -terminated surfaces (Fig. 4a). These surfaces were optimized structurally and the electronic structures of the reconstructed surfaces were investigated. Both the two O-terminated surfaces resulted in an insulating band structure (Fig. S3a,b), which is inconsistent with the experimental tunneling spectra (Fig. 2). For the Kagome-lattice Ti-terminated surface, the simulated charge density plot (Fig. S3c) also show inconsistency with the experimental topographic image (Fig. 1). Consequently, neither the O-terminated nor the Kagome-lattice Ti-terminated surface reproduced the experimental results (Fig. S3).

We next investigated the TiLi_2 -terminated surface, and further examined the effect of Li deficiency on the electronic structures (TiLi_{2-x} -terminated surface). The TiLi_2 -terminated surface contains a triangular lattice of Ti atoms, and two types of Li atoms: Li atoms displaced

toward the vacuum (hereafter called higher Li atoms, dark green circle in Fig. 4a) and those displaced toward the bulk (hereafter called lower Li atoms, light green circle in Fig. 4a). We studied three types of models for this TiLi_{2-x} -terminated surface: a stoichiometric TiLi_2 -terminated surface, a surface without the higher Li atoms (TiLi_1 -terminated surface), and a surface without both higher and lower Li atoms (TiLi_0 -terminated surface) (Fig. 4b). These surfaces were considered because Li may be deficient during depositions because of its high volatility. We show the simulated electron charge density of the optimized surfaces represent high intensity spots centered on the Ti sites (Fig. 4c). The result is a consequence of the dominant DOS contribution from Ti 3d orbitals near E_F , and the impact of Li atoms is expected to be negligible in the STM images; Li atoms are strongly ionized and contribute little in STM images. Thus, the protrusions of the triangular lattice seen in the topographic image (Fig. 1a) can be well-explained by Ti atoms on the surface. Based on above discussions, we conclude that the surface of a LiTi_2O_4 (111) film is terminated with TiLi_{2-x} .

We now compare the DOS at E_F , $N(E_F)$, of a bulk and that of a TiLi_{2-x} -terminated surfaces, and reveal that the surfaces have smaller $N(E_F)$ than that of the bulk. Our DFT calculations for *bulk* show a peak structure at E_F (Fig. 4d), which is consistent with previous calculations using the linear muffin-tin orbital method⁴⁶ and full-potential linearized augmented-plane-wave⁴⁷. The simulated peak structure at E_F is also consistent with an experimental report of large normal state electronic specific heat, which is a measure of $N(E_F)$ for *bulk*³⁷. On the TiLi_{2-x} -terminated surface (Fig. 4e), a broken lattice symmetry normal to the surface lifts the degeneracy of the t_{2g} orbitals and modifies the orbital states on the surface. Importantly, compared with bulk, we observed 15%, 20%, and 45% reduction of the DOS at the topmost Ti atoms for TiLi_2 , TiLi_1 , and TiLi_0 , respectively (Fig. 4e). Because the smaller $N(E_F)$ leads to lower T_c according to the

BCS theory, the calculations suggest that T_c is suppressed on the surface.

Based on the above discussions, we interpret the experimental results. Indeed, as the calculation predicted, we experimentally observed a characteristic pseudogap structure near E_F in the tunneling spectra, in the energy range of $-100 \text{ meV} < E < + 50 \text{ meV}$ (shaded red in Fig. 2a), strongly supporting the emergence of the T_c -suppressed layer on the surface. Given that the present $2\Delta/k_B T_c \sim 3.0$ was calculated using bulk T_c (13 K), the small $2\Delta/k_B T_c$ value is explained from a suppressed T_c on the surface. If we assume the $2\Delta/k_B T_c$ value as 3.52, which is a typical value in the weak coupling limit for BCS superconductors, T_c is evaluated at ~ 11 K. The large ξ value is also in line with the presence of a T_c -suppressed layer due to following discussion. The Fermi velocity v_F is proportional to $1/N(E_F)$; therefore, the reduced number $N(E_F)$ leads to an increase in v_F on the surface. Thus, the large v_F value on a surface increases ξ based on the formula $\xi = v_F/\Delta$ derived from BCS theory.

Finally, we briefly point out a possible additional origin for a pseudogap formation, a charge ordering near surfaces. The charge ordering has been observed in a wide variety of mixed valence charge frustrated systems⁴⁸⁻⁵⁵. Because LiTi_2O_4 can be regarded as a mixed-valence charge frustrated $3d^{0.5}$ system $\{\text{Ti}^{3+} (3d^0 \text{ with } S=0) \text{ and } \text{Ti}^{4+} (3d^1 \text{ with } S=1/2)\}$, charges tend to order in this system. While the charge ordering and pseudogap formation have not been reported previously in *bulk* LiTi_2O_4 , the observed pseudogap might be induced from a charge ordering assisted by such surface effects as electronic and structural reconstruction, and/or surface phonon effects^{56,57}. In particular, in the present (111) plane, the Kagome and triangular lattices of the Ti atoms provide a 2D frustration network, which may also lead to a *frustrating* spin state^{50,51,58} driven by charge *ordering* near surfaces.

In summary, we have investigated superconductivity in the atomically well-defined surface of $\text{LiTi}_2\text{O}_4(111)$ thin films, using STM/STS and first-principles calculations. We provided spectroscopic evidence of modified superconductivity on the surface, originating from the formation of a pseudogap in the DOS. The study has made an essential first step towards exploring superconducting phenomena emerging from inherent atomic and electronic *reconstruction* on a *surface* of superconducting cubic transition-metal oxides.

Methods

Samples and characterizations. We used a low-temperature scanning tunneling microscope connected with a pulsed laser deposition (PLD) chamber. This system enables us to investigate thin-film surfaces immediately after their deposition, without exposing surfaces to air. The base pressure of the PLD chamber was 5×10^{-11} Torr. Thin films of LiTi_2O_4 are grown on Nb(0.05 wt %)-doped SrTiO_3 (111) substrate using PLD with a KrF excimer laser (wavelength $\lambda = 248$ nm) and $\text{Li}_4\text{Ti}_5\text{O}_{12}$ as a target. Substrates were annealed at 1000°C for an hour in oxygen under a partial pressure $P_{\text{O}_2} = 5 \times 10^{-7}$ Torr before film depositions. Substrates were resistively heated, and their temperatures were monitored using a pyrometer. We deposited film at a substrate temperature $T_s = 300^\circ\text{C}$ under $P_{\text{O}_2} = 5 \times 10^{-7}$ Torr followed by post-deposition annealing at 600°C in UHV for one hour. During thin film depositions, pulse repetition and fluence were set at 2 Hz and 1 J/cm^2 , respectively. Film thickness, measured *ex situ* using a DEKTAK 3030ST mechanical profiler, was determined to be about 100 nm. All STM experiments were performed at liquid-He temperature (4.2 K). For *ex situ* characterization, we measured X-ray diffraction pattern and temperature dependence of magnetization after *in situ* STM/STS measurements.

First principles calculations. For the first-principles calculations, we used DFT with the code *Quantum ESPRESSO*, with the generalized gradient approximation and ultra-soft pseudopotential scheme^{59–63}. Cutoff energies for the Kohn–Sham orbitals and charge density of 32.5 Ry and 45 Ry are imposed. The Brillouin-zone summation is evaluated using a $3\times 3\times 1$ k-point sampling. Convergence criteria of the structure optimization are 10×10^{-3} for forces and 10×10^{-4} for energy. For the calculation of the near surface atomic/electronic structures, we use the symmetric slab model with 4 unit cells along the (111) direction on each side. In the structure optimization, the topmost surface structures are initiated from bulk cuts. The atomic positions of the Ti atoms at the center of the symmetric slab model along the (111) direction are fixed during optimization. Spin degrees of freedom and electron–electron correlations are not included in the calculation.

Acknowledgement

We thank Y. Takagi and K. Yamamoto for experimental assistance, and T. Hanaguri, T. Machida, Y. Yoshida, H. Kawasoko, and K. Sato for useful discussions. Y. O. acknowledges funding from JSPS KAKENHI Grant Nos. 26707016 and 25886004. T. H. acknowledges funding from JSPS KAKENHI Grant Nos. 26246022, 26106502, 26108702, 26610092, JST-PRESTO, and JST-CREST program. This work was supported by the World Premier Research Center Initiative (WPI), promoted by the Ministry of Education, Culture, Sports, Science and Technology (MEXT) of Japan.

Author Contributions

Y. O. pursued film growth, STM/STS measurements, and data analysis. Y. A performed the first-principles calculations. Y. O., R. S., S. S., and T. H. discussed the experimental results. Y. A., E. M., and S. W. discussed the theoretical calculations. All authors discussed the conclusions of this paper. Y. O. and T. H. wrote the paper.

References

1. Bozovic, I., Logvenov, G., Belca, I., Narimbetov, B. & Sveklo, I., Epitaxial Strain and Superconductivity in $\text{La}_{2-x}\text{Sr}_x\text{CuO}_4$ Thin Films. *Phys. Rev. Lett.* **89**, 107001 (2002).
2. Gozar, A., Logvenov, G., Fitting Kourkoutis, L., Bollinger, A. T., Giannuzzi, L. A., Muller, D. A. & Bozovic, I., High-temperature interface superconductivity between metallic and insulating copper oxides. *Nature* **455**, 782–785 (2008).
3. Bert, J. A., Kalisky, B., Bell, C., Kim, M., Hikita, Y., Hwang, H. Y. & Moler, K. A. Direct imaging of the coexistence of ferromagnetism and superconductivity at the $\text{LaAlO}_3/\text{SrTiO}_3$ interface. *Nat. Phys.* **7**, 767–771 (2011).
4. Li, L., Richter, C., Mannhart, J. & Ashoori, R. C., Coexistence of magnetic order and two-dimensional superconductivity at $\text{LaAlO}_3/\text{SrTiO}_3$ interfaces. *Nat. Phys.* **7**, 762–766 (2011)
5. Scheurer, M. S. & Schmalian, J., Topological superconductivity and unconventional pairing in oxide interfaces. *Nat. Commun.* **6**, 6005 (2014).
6. Gor'kov, L. P. & Rashba, E. I., Superconducting 2D System with Lifted Spin Degeneracy: Mixed Singlet-Triplet State. *Phys. Rev. Lett.* **87** 037004 (2001).
7. Liu, D. *et al.*, Electronic origin of high-temperature superconductivity in single-layer FeSe superconductor. *Nat. Commun.* **3**, 931 (2012).
8. Ge, J. F. *et al.* Superconductivity above 100 K in single-layer FeSe films on doped SrTiO_3 . *Nat. Mater.* **14**, 285–289 (2015).
9. Shiogai, J., Ito, Y., Mitsuhashi, T., Nojima, T. & Tsukazaki, A., Electric-field-induced superconductivity in electrochemically etched ultrathin FeSe films on SrTiO_3 and MgO. *Nat. Phys.* **12**, 42–46 (2016).
10. Miyata, Y., Nakayama, K., Sugawara, K., Sato, T. & Takahashi, T., High-temperature superconductivity in potassium-coated multilayer FeSe thin films. *Nat. Mater.* **14**, 775–779

- (2015).
11. Guo, Y., Zhang, Y. F., Bao, X. Y., T. Z. Han, Tang, Z., Zhang, L. X., Zhu, W. G., Wang, E. G., Niu, Q., Qiu, Z. Q., J. F. Jia, Zhao, Z. X. & Xue, Q. K., Superconductivity Modulated by Quantum Size Effects. *Science* **306**, 1915 (2004).
 12. Qin, S., Kim, J., Niu, Q. & Shih, C. K., Superconductivity at the Two-Dimensional Limit *Science* **324**, 1314–1317, (2009).
 13. Nishio, T., Ono, M., Eguchi, T., Sakata, H. & Hasegawa, Y., Superconductivity of nanometer-size Pb islands studied by low-temperature scanning tunneling microscopy. *Appl. Phys. Lett.* **88**, 113115 (2006).
 14. Zhang, T., Cheng, P., Li, W. J., Sun, Y. J., Wang, G., Zhu, X. G., He, K., Wang, L., Ma, X., Chen, X., Wang, Y., Liu, Y., Lin, H. Q., Jia J. F., & Xue, Q. X., Superconductivity in one-atomic-layer metal films grown on Si(111). *Nat. Phys.* **6** 104 (2010).
 15. Uchihashi, T., Mishra, P., Aono, M. & Nakayama, T., Macroscopic Superconducting Current through a Silicon Surface Reconstruction with Indium Adatoms: Si(111)-(√7×√3)-In. *Phys. Rev. Lett.* **107**, 207001 (2011).
 16. Yoshizawa, S., Kim, H., Kawakami, T., Nagai, Y., Nakayama, T., Hu, X., Hasegawa, Y. & Uchihashi, T., Imaging Josephson Vortices on the Surface Superconductor Si(111)-(√7×√3)-In using a Scanning Tunneling Microscope. *Phys. Rev. Lett.* **113**, 247004 (2014).
 17. Brun, C., Cren, T., Cherkez, V., Debontridder, F., Pons, S., Fokin, D., Tringides, M. C., Bozhko, S., Ioffe, L. B., Altshuler, B. L. & Roditchev, D., Remarkable effects of disorder on superconductivity of single atomic layers of lead on silicon. *Nat. Phys.* **10**, 444–450 (2014).
 18. Joe, Y. I., Abbamonte, P. & Geck, J., Orbital textures and charge density waves in transition-

- metal dichalcogenides. *Nat. Phys.* **11**, 328–331 (2015)
19. Xi, X., Wang, Z., Zhao, W., Park, J. H., Law, K. T., Berger, H., Forró, L., Shan, J. & Mak, K. F., Ising pairing in superconducting NbSe₂ atomic layers. *Nat. Phys.* **12**, 139–143 (2016)
 20. Lu, J. M., Zheliuk, O., Leermakers, I., Yuan, N. F. Q., Zeitler, U., Law, K. T. & Ye, J. T., Evidence for two-dimensional Ising superconductivity in gated MoS₂. *Science* **350**, 1353–1357 (2015).
 21. Lee, S., Takagi, H., Louca, D., Matsuda, M., Ji, S., Ueda, H., Ueda, Y., Katsufuji, T., Chung, J. H., Park, S., Cheong, S. W., & Broholm, C., Frustrated Magnetism and Cooperative Phase Transitions in Spinel. *J. Phys. Soc. Japan* **79**, 011004 (2010).
 22. Jin, K., He, G., Zhang, X., Maruyama, S., Yasui, S., Suchoski, R., Shin, J., Jiang, Y., Yu, H.S., Shan, L., Greene, R. L. & Takeuchi, I., Anomalous magnetoresistance in the spinel superconductor LiTi₂O₄. *Nat. Commun.* **6**, 7183 (2015).
 23. Bragg, W., The structure of magnetite and the spinels. *Nature* **95** 561–561 (1915)
 24. Johnston, D. C., Prakash, H., Zachariasen, W. H., High Temperature Superconductivity in Li-Ti-O Ternary System. *Mat. Res. Bull.* Vol. **8**, 777–784, (1973).
 25. Johnston, D. C., Superconducting and Normal State Properties of Li_{1+x}Ti_{2-x}O₄ Spinel Compounds. I. Preparation, Crystallography, Superconducting Properties, Electrical Resistivity, Dielectric Behavior, and Magnetic Susceptibility. *J. Low Temp. Phys.* **25**, 145 (1976).
 26. Callum, R. W., Johnston, D. C., Luengo, C. A., & Maple, M. P., Superconducting and normal state properties of Li_{1+x}Ti_{2-x}O₄ spinel compounds. II. Low-temperature heat capacity. *J. Low Temp. Phys.* **25**, 177 (1976).
 27. Robbins, M., Willens, R.H., & Miller, R.C., Superconductivity in the spinels CuRh₂S₄ and CuRh₂Se₄. *Solid State Commun.* **5**, 933 (1967).

28. Shelton, R. N., Johnston, D. C., & Adrian, H., Measurement of the pressure dependence of T_c for superconducting spinel compounds. *Solid State Commun.* **20**, 1077 (1976).
29. Hagino, T., Seki, Y., Wada, N., Tsuji, S., Shirane, T., Kumagai, K., & Nagata, S., Superconductivity in spinel-type compounds CuRh_2S_4 and CuRh_2Se_4 . *Phys. Rev. B* **51**, 12673 (1995).
30. Ito, M., Hori, J., Kurisaki, H., Okada, H., Kuroki, A. J. P., Ogita, N., Udagawa, M., Fujii, H., Nakamura, F., Fujita, T., & Suzuki, T., Pressure-Induced Superconductor-Insulator Transition in the Spinel Compound CuRh_2S_4 . *Phys. Rev. Lett.* **91** 077001(2003).
31. Cao, G., Furubayashi, T., Suzuki, H., Kitazawa, H., Matsumoto, T., & Uwatoko, Y., Suppression of metal-to-insulator transition and appearance of superconductivity in $\text{Cu}_{1-x}\text{Zn}_x\text{Ir}_2\text{S}_4$. *Phys. Rev. B* **64**, 214514 (2001).
32. Luo, H., Klimczuk, T., MÜchler, L., Schoop, L., Hirai, D., Fuccillo, M. K., Felser, C., & Cava, R. J., Superconductivity in the $\text{Cu}(\text{Ir}_{1-x}\text{Pt}_x)_2\text{Se}_4$ Spinel. *Phys. Rev. B* **87**, 214510 (2013).
33. Ng, K. W. Khim, Z. G. Shum, D. P. & Wolf, E. L., Vacuum Tunneling Spectroscopy of This Film and Bulk Polycrystalline Superconductors. *Surface Science* **181**, 37–45 (1987).
34. Ekino, T., & Akimitsu, J., Superconducting energy gap in spinel compound $\text{Li}_{1+x}\text{Ti}_{2-x}\text{O}_4$ from electron tunneling. *Physica B* **165**, 1599 (1990).
35. Sun, C. P., Lin, J.-Y., Mollah, S., Ho, P. L., Yang, H. D., Hsu, F. C., Liao, Y. C., & Wu, M. K., Magnetic field dependence of low-temperature specific heat of the spinel oxide superconductor LiTi_2O_4 . *Phys. Rev. B* **70**, 054519 (2004).
36. Tang, L., Zou, P. Y., Shan, L., Dong, A. F., Che, G. C., & Wen, H. H., Electrical resistivity and Andreev reflection spectroscopy of the superconducting oxide spinel LiTi_2O_4 . *Phys. Rev. B* **73**, 184521 (2006).

37. Tunstal, D. P., Todd, J. R. M., Arumugam, S., Dai, G., Dalton, M. & Edwards, P. P., Titanium nuclear magnetic resonance in metallic superconducting lithium titanate and its lithium-substituted derivatives $\text{Li}_{1+x}\text{Ti}_{2-x}\text{O}_4$ ($0 < x < 0.10$). *Phys. Rev. B* **50**, 16541–16549 (1994).
38. Chopdekar, R. V., Wong, F. J., Takamura, Y., Arenholz, E. & Suzuki, Y., Growth and characterization of superconducting spinel oxide LiTi_2O_4 thin films. *Physica C* **469**, 1885–1891 (2009).
39. Kumatani, A., Ohsawa, T., Shimizu, R., Takagi, Y., Shiraki, S. & Hitosugi, T., Growth processes of lithium titanate thin films deposited by using pulsed laser deposition. *Appl. Phys. Lett.* **101**, 123103 (2012).
40. Oshima, T., Niwa, M., Yokoyama, K., & Ohtomo, A., Pulsed-laser deposition of superconducting LiTi_2O_4 ultrathin films. *J. Crystal Growth*, **419**, 153–157 (2015).
41. Iwaya, K., Shimizu, R., Hashizume, T., & Hitosugi, T., Systematic analyzes of vibration noise of a vibration isolation system for high-resolution scanning tunneling microscopes. *Rev. Sci. Instrum.* **82**, 083702 (2011).
42. Dynes, R. C., Narayanamurti, V. & Garno, J. P., Direct Measurement of Quasiparticle-Lifetime Broadening in a Strong-Coupled Superconductor. *Phys. Rev. Lett.* **41** 1509 (1978)
43. Song, C. L., Wang, Y. L., Jiang, Y. P., Wang, L., He, K., Chen, X., Hoffman, J. E., Ma, X. C. & Xue, Q. K., Suppression of Superconductivity by Twin Boundaries in FeSe. *Phys. Rev. Lett.* **109**, 137004 (2012).
44. Chopdekar, R. V., Wong, F. J., Takamura, Y., Arenholz, E. & Suzuki, Y., Growth and characterization of superconducting spinel oxide LiTi_2O_4 thin films. *Physica C* **469**, 1885–1891 (2009).
45. Song, C. L., Yin, Y., Zech, M., Williams, T., Yee, M. M., Chen, G. F., Luo, J. L., Wang, N.

- L., Hudson, E. W. & Hoffman, J. E., Dopant clustering, electronic inhomogeneity, and vortex pinning in iron-based superconductors. *Phys. Rev. B* **87**, 214519 (2013).
46. Satpathy, S. & Martini, R. M., Electronic structure of the superconducting oxide spinel LiTi_2O_4 . *Phys. Rev. B* **36**, 7269 (1987).
47. Massidda, S., Yu, J. & Freeman, A. J., Electronic structure and properties of superconducting LiTi_2O_4 . *Phys. Rev. B* **38**, 11352 (1988).
48. Irizawa, A., Shimai, K., Sato, K., Iizuka, K., Nishiyama, M., Nanba, T., Niitaka, S. & Takagi, H., Observation of charge ordering state in LiV_2O_4 investigated by optical study. *J. Phys.: Conference Series* **150**, 042070 (2009).
49. Irizawa, A., Suga, S., Isoyama, G., Shimai, K., Sato, K., Iizuka, K., Nanba, T., Higashiya, A., Niitaka, S. & Takagi, H., Direct observation of a pressure-induced metal-insulator transition in LiV_2O_4 by optical studies. *Phys. Rev. B* **84**, 235116 (2011).
50. Matsuno, K., Katsufuji, T., Mori, S., Moritomo, Y., Machida, A., Nishibori, E., Takata, M., Sakata, M., Yamamoto, N. & Takagi, H., Charge Ordering in the Geometrically Frustrated Spinel AlV_2O_4 . *J. Phys. Soc. Jpn.* **70**, 1456 (2001).
51. Matsuno, K., Katsufuji, T., Mori, S., Nohara, M., Machida, A., Moritomo, Y., Kato, K., Nishibori, E., Takata, M., Sakata, M., Kitazawa, K. & Takagi, H., Charge Ordering and Spin Frustration in $\text{AlV}_{2-x}\text{Cr}_x\text{O}_4$. *Phys. Rev. Lett.* **90**, 096404 (2003).
52. Kasuya, Y. & Tsunoda, Y., Charge and spin ordering in LiMn_2O_4 . *Phys. Rev. B* **64**, 094422 (2001).
53. Senn, M. S. & Attfield, J. P., Charge order and three-site distortions in the Verwey structure of magnetite. *Nature* **481**, 173 (2012).
54. Radaelli, P. G., Horibe, Y., Gutmann, M. J., Ishibashi, H., Chen, C. H., Ibberson, R. M., Koyama, Y., Hor, Y. S., Kiryukhin, V. & Cheong, S. W., Formation of isomorphic Ir^{3+} and

- Ir^{4+} octamers and spin dimerization in the spinel CuIr_2S_4 , *Nature* **416**, 155–158 (2002).
55. Takubo, K., Hirata, S., Son, J.-Y., Quilty, J.W., Mizokawa, T., Matsumoto, N. & Nagata, S., X-Ray Photoemission Study of CuIr_2S_4 : Ir^{3+} - Ir^{4+} Charge Ordering and the Effect of Light Illumination. *Phys. Rev. Lett.* **95**, 246401 (2005).
56. Itoh, Y., Moritsu, N. & Yoshimura, K., Emergence of antiferromagnetic correlation in $\text{LiTi}_{2-x}\text{V}_x\text{O}_4$ via ^7Li NMR. *J. Phys. Soc. Jpn.* **77**, 123713 (2008).
57. Tunstal, D. P., Todd, J. R. M., Arumugam, S., Dai, G., Dalton, M. & Edwards, P. P., Titanium nuclear magnetic resonance in metallic superconducting lithium titanate and its lithium-substituted derivatives $\text{Li}_{1+x}\text{Ti}_{2-x}\text{O}_4$ ($0 < x < 0.10$). *Phys. Rev. B* **50**, 16541–16549 (1994).
58. Carpinelli, J. M., Weitering, H. H., Plummer, E. W., & Stumpf, R., Direct observation of a surface charge density wave. *Nature* **381**, 398–400 (1996).
59. Giannozzi, P. *et al.*, Quantum espresso. *J. Phys. Condens. Matter* **21**, 395502 (2009).
60. Hohenberg, P., Kohn, W., Inhomogeneous Electron Gas. *Phys. Rev. B* **136**, B864 (1964).
61. Kohn W., & Sham, L. J., Self-Consistent Equations Including Exchange and Correlation Effects. *Phys. Rev.* **140**, 1133 (1965).
62. Vanderbilt, D., Soft self-consistent pseudopotentials in a generalized eigenvalue formalism. *Phys. Rev. B* **41**, 7892 (1990).
63. Perdew, J. P., Burke, K., & Ernzerhof, M., Generalized Gradient Approximation Made Simple. *Phys. Rev. Lett.* **77**, 3865 (1996).

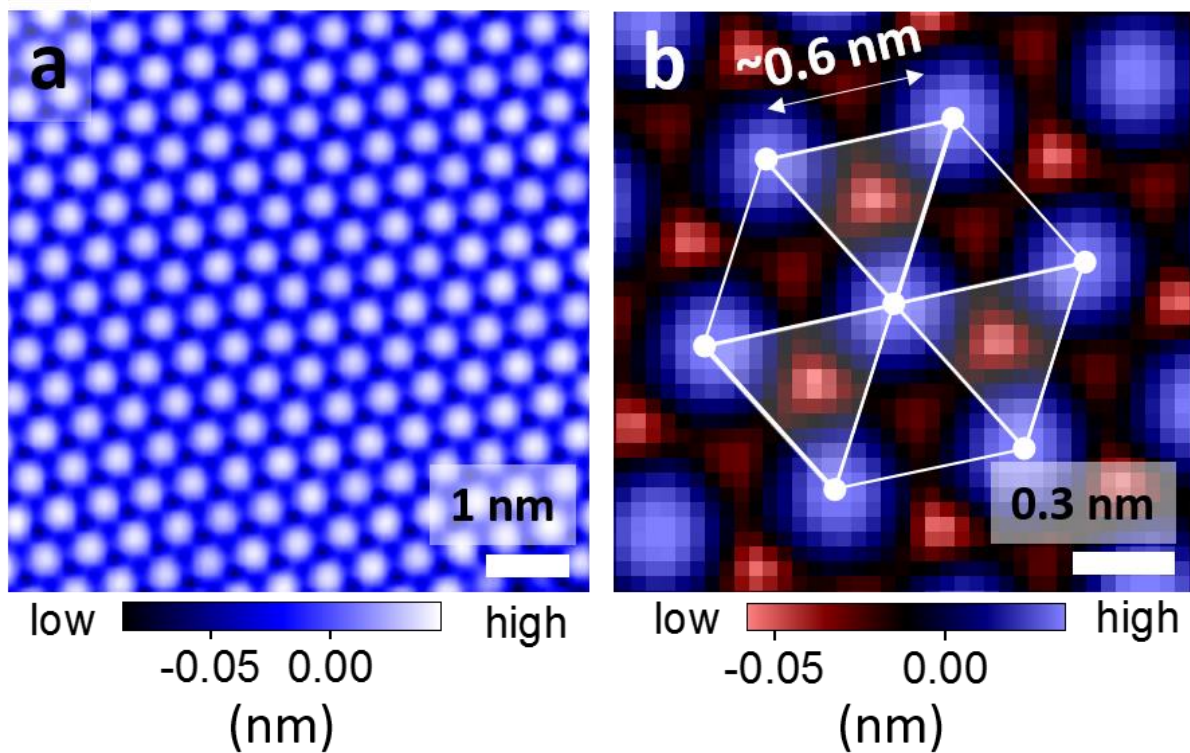


Figure 1 | Typical topographic images on a terrace. (a) Scanning tunneling microscope image of LiTi₂O₄ (111) surface (7 nm × 7 nm). **(b)** Close-up image (1.7 nm × 1.7 nm) of **a**. Both images are obtained with a sample bias voltage of +30 mV and a tunneling current of 30 pA.

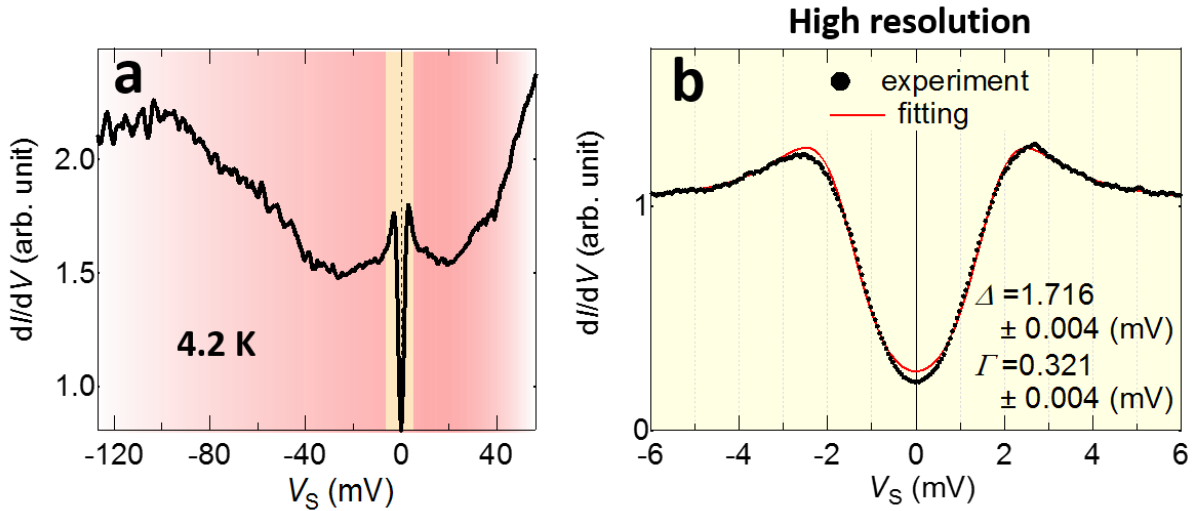


Figure 2 | Tunneling spectra obtained at 4.2 K. (a) Tunneling spectrum obtained at a wide energy region (sample bias voltages of -130 mV to $+50$ mV). Superconducting gap (energy region shaded in yellow) is observed. Note that the superconducting gap appears inside the pseudo-gap formed at around -100 mV to $+50$ mV (energy region shaded with red). (b) High-resolution tunneling spectrum for voltages between ± 6 mV near the Fermi energy. Experimental curve (black dots) and fitted curve (red line) are shown in the same figure. See main body for the details of the fitting procedure. The energy resolutions for the spectra of **a** and **b** are 1.5 mV and 0.3 mV, respectively.

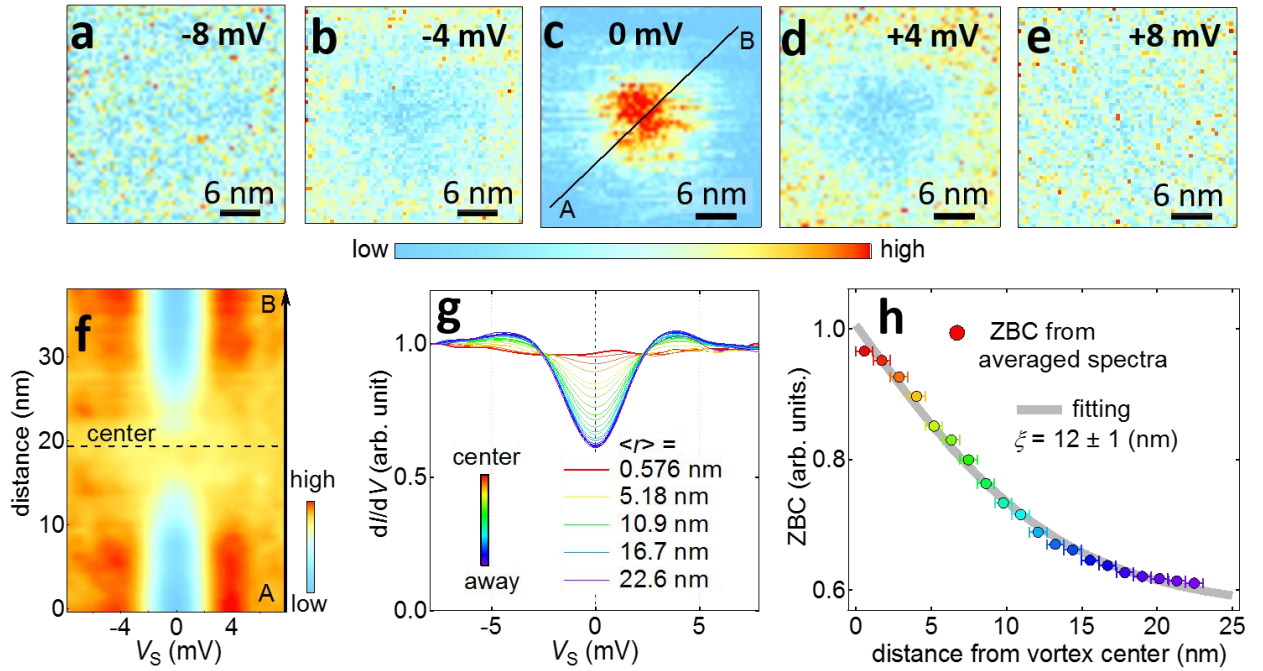


Figure 3 | Spectral evolution around a single vortex core (temperature of 4.2 K, magnetic field of 1.5 T normal to the surface). (a–e) Conductance mappings around an isolated single vortex core with various sample bias voltages. A scanning tunneling microscope tip is stabilized at a tunneling current of 30 pA and a sample bias voltage of -10 mV. The energy resolution is set at 1 mV. (f) Spatial evolution of tunneling spectra across the vortex center (the line is shown in c). (g) Averaged spectra as function of distance from vortex center $\langle r \rangle$. (h) Zero bias conductance (ZBC) obtained from g. Coherence length of ~ 12 nm is obtained by fitting the ZBC (see main text for details).

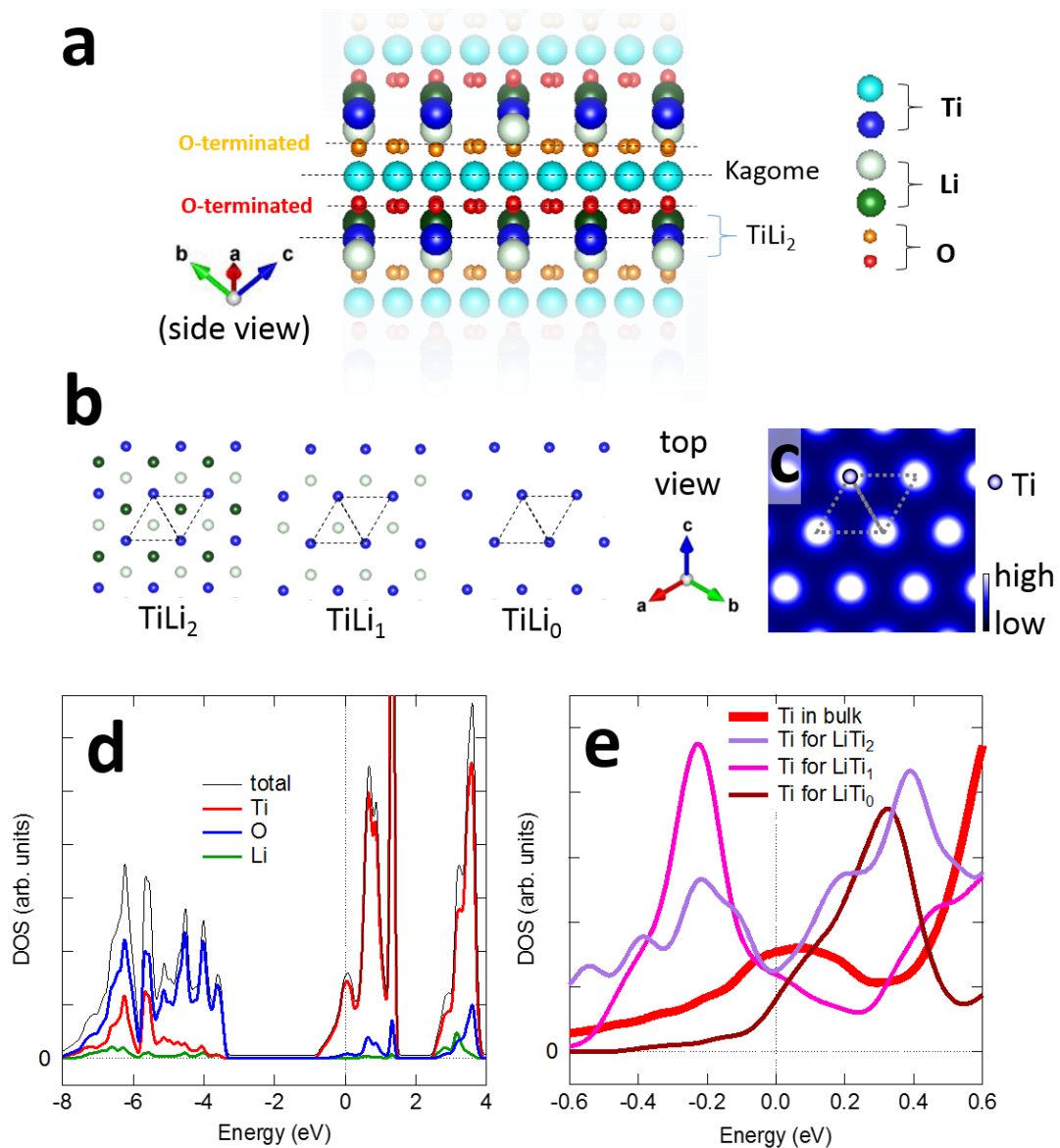


Figure 4 | Comparison between bulk and surface electronic states based on DFT. (a) Crystal structure with bulk continuum, together with four bulk-cut planes represented by broken lines. Vertical axis is along the (111) crystal orientation. (b) Top view for TiLi_{2-x} terminated surfaces: TiLi_2 (left), TiLi_1 (middle), and TiLi_0 (right). (c) Charge density plot at the Fermi energy for the top-most atomic layer of LiTi_0 (right in b). Dotted lines in b and c indicate the unit cell on the surface. (d) Calculated density of states (DOS) for bulk LiTi_2O_4 . (e) Calculated DOS for the top-most Ti atoms in TiLi_{2-x} layer. Here, 0 on the horizontal axes in d and e correspond to the Fermi energy.

Supplementary Information

Scanning tunneling spectroscopy of superconductivity on surfaces of $\text{LiTi}_2\text{O}_4(111)$ thin films

Yoshinori Okada¹, Yasunobu Ando², Ryota Shimizu¹, Emi Minamitani², Susumu Shiraki¹, Satoshi
Watanabe² & Taro Hitosugi^{1,3}

¹Advanced Institute for Materials Research, Tohoku University, Sendai 980-8577, Japan

²Department of Materials Engineering, The University of Tokyo, Tokyo 113-8656, Japan

³School of Materials and Chemical Technology, Tokyo Institute of Technology, Tokyo 152-8552,
Japan

Supplementary Figures

Figure S1 | *Ex situ* characterization of the film using X-ray diffraction (XRD) and magnetic measurements.

Figure S2 | Procedures to analyze zero-bias conductance.

Figure S3 | Results of density functional theory (DFT) calculations.

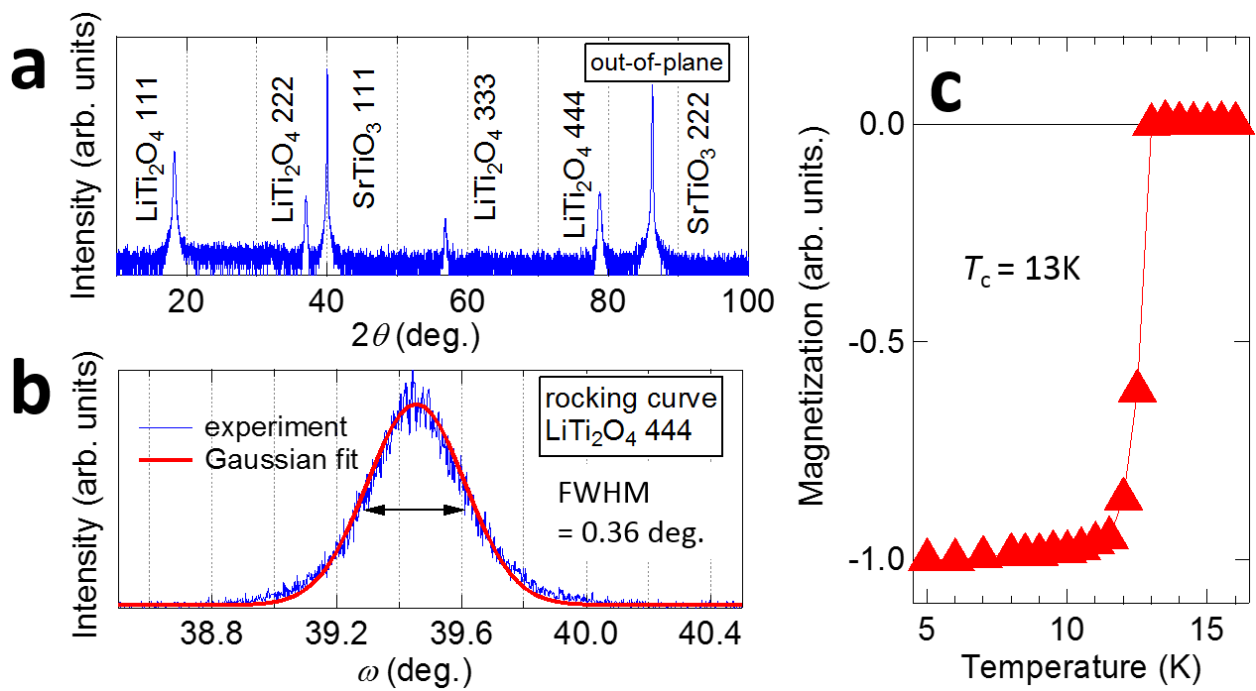


Figure S1 | *Ex situ* characterization of film using X-ray diffraction (XRD) and magnetic measurements. (a) Out-of-plane XRD pattern of a LiTi_2O_4 film on a $\text{SrTiO}_3(111)$ substrate. (b) Rocking curve of the 444 peak. The full-width at half maximum (FWHM) value was $\sim 0.36^\circ$. Intensities in **a** and **b** are given in logarithmic and linear scale, respectively. (c) Temperature dependence of the magnetization of the LiTi_2O_4 film shown in (a). Superconducting transition temperature T_c was ~ 13 K.

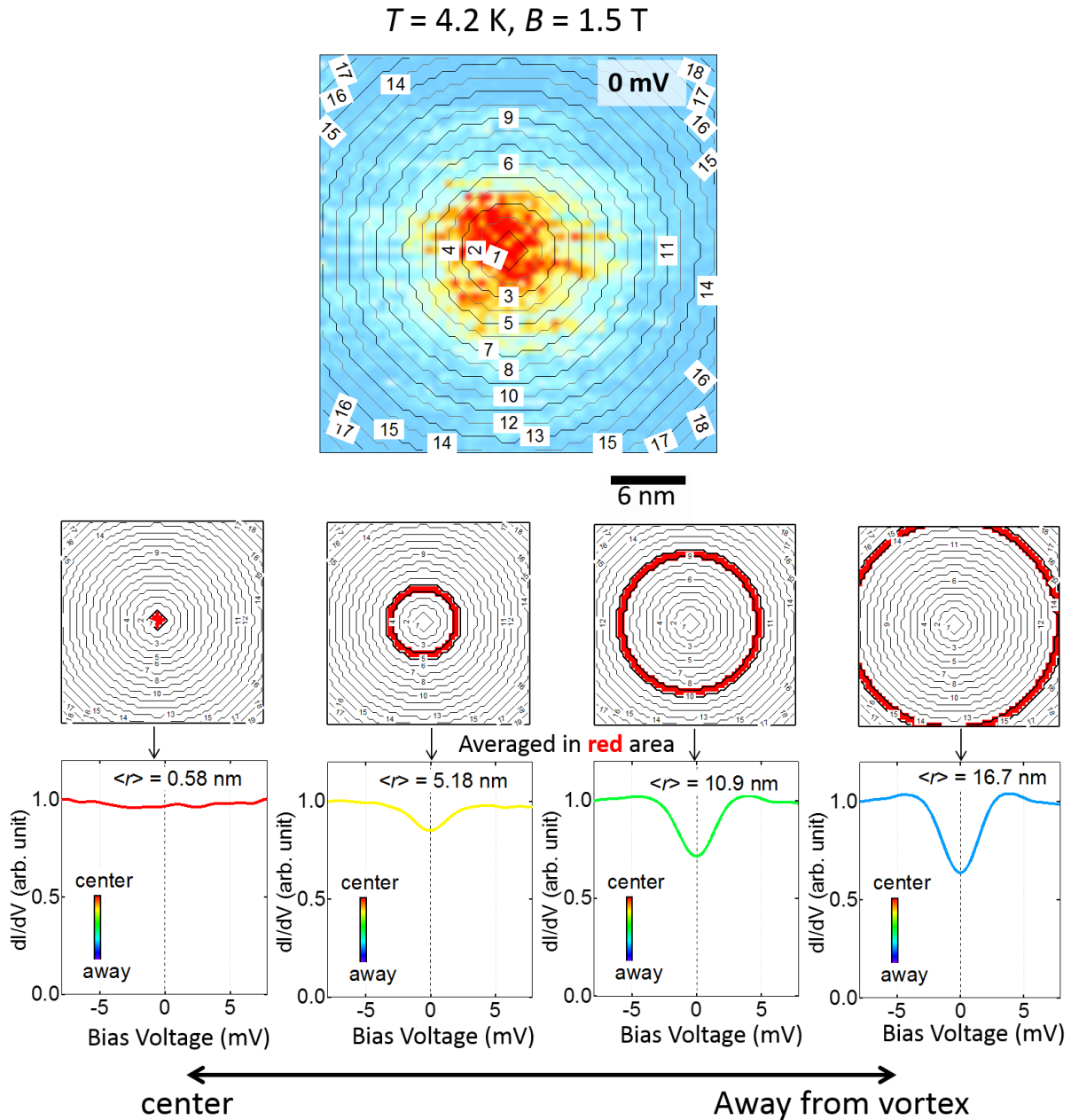


Figure S2 | Procedures to analyze zero-bias conductance. To determine the center of a vortex, we first fit the zero-bias conductance mapping (Fig. 3c) with a 2D Gaussian. Then, using concentric circles around the vortex center (top), we classified the data shown in Fig. 3a–e into 20 regions. We averaged spectra within the regions, and the series of spectra were obtained from closest (red in Fig. 3h) to farthest (purple in Fig. 3h) from the vortex center. We show four examples of the regions (marked in red) together with the averaged spectra obtained within the regions. The data were obtained at a temperature T and magnetic field B of 4.2 K and 1.5 T, respectively.

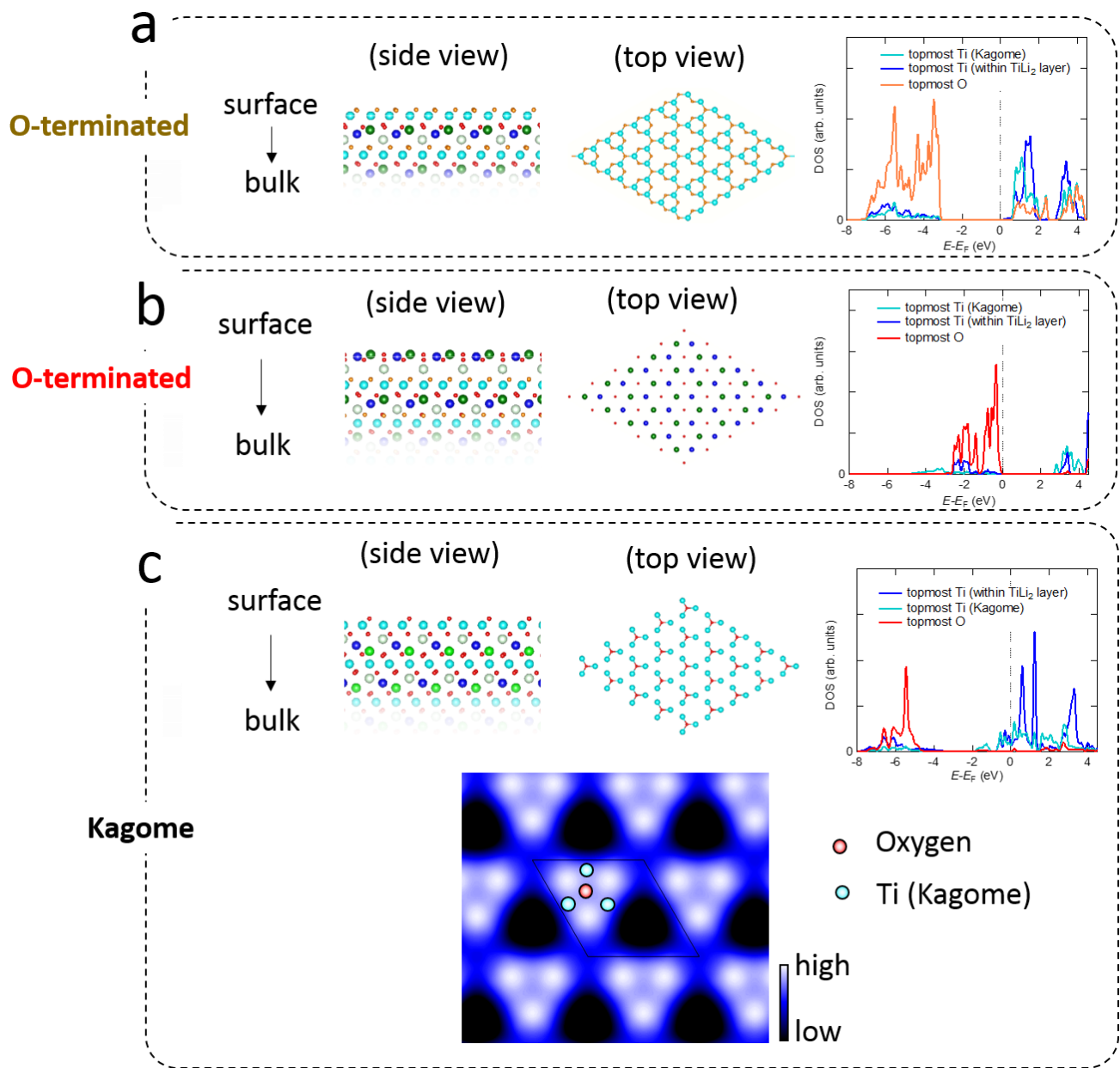


Figure S3 | Results of density functional theory (DFT) calculations. (a–b) Optimized near surface structures (left) and partial density of states (right) for two O-terminated bulk cuts in Fig. 4a. The results clearly show that these models exhibit insulating electronic structure on the surface, which is inconsistent with experimental metallic tunneling spectra (Fig. 2). (c) Optimized near surface structures (left) and partial density of states (upper right) for Kagome-lattice Ti-terminated bulk cut in Fig. 4a. Bottom image shows a Tersoff–Hamann simulated charge density plot at $E - E_F = 0$ eV at 0.2 nm above the topmost oxygen atom, but does not reproduce the experimental results of Fig. 1.